Journal of Power Sources 195 (2010) 2905–2908

Contents lists available at ScienceDirect

Journal of Power Sources

journal homepage: www.elsevier.com/locate/jpowsour

Short communication

The superior lithium storage capabilities of ultra-fine rutile TiO_2 nanoparticles

Jun Song Chen, Xiong Wen Lou *

School of Chemical and Biomedical Engineering, Nanyang Technological University, 70 Nanyang Drive, Singapore 637457, Singapore

ARTICLE INFO

Article history:
Received 15 October 2009
Received in revised form 9 November 2009
Accepted 9 November 2009
Available online 14 November 2009

Keywords:
Titanium dioxide
Rutile
Ultra-fine
High-power anode
Lithium-ion batteries

ABSTRACT

The lithium storage capabilities of ultra-fine rutile TiO_2 nanoparticles have been studied. Ultra-fine rutile TiO_2 nanoparticles with only several nanometers in size have been prepared by a modified wet-chemical method with a high yield. Unexpectedly, the rutile TiO_2 nanoparticles with 3 nm in size exhibit superior lithium storage properties. Specifically, they show long term cycling stability upon extended cycling for at least 300 cycles with a capacity loss of only 0.17% per cycle, and good rate capability up to a 30 C rate. The excellent reversible lithium storage capabilities could be attributed to the ultra-fine size giving rise to a very short diffusion path, and the relatively large surface area which provides more sites for lithium insertion.

1. Introduction

Nanostructured materials are intensively studied as electrode materials for lithium-ion batteries (LIB) [1–10]. Titanium oxide (TiO_2) is a good candidate for high-power anodes because of its low-cost, ready availability in large scale, and environmental benignity [4,11–13]. Among all the TiO_2 polymorphs, anatase is generally considered as the most electroactive host for lithium insertion, while the rutile counterpart is said to be only able to intercalate negligible amount of lithium at room temperature [14–19]. A lot of efforts have been devoted to understand the nature of lithium insertion into the rutile crystal structure [13,15,19–21]. It has been found that Li insertion into microsized rutile particles is kinetically restricted at room temperature [22,23], and full insertion is only possible at 120 °C [24]. This is largely due to the highly anisotropic diffusion of Li^+ ions in the rutile 3D crystal structure. Specifically, the tetragonal rutile is composed of TiO_6 octahedra which share edges along the *c*-direction and corners in the *ab*-plane [21]. In order to reach the preferred insertion sites at the oxygen octahedral vacancy [25], Li^+ ions have to migrate through the *ab*-plane. However, the diffusion coefficient for Li^+ along the *ab*-plane is only 10^{-15} cm^2 s^{-1}, which is 9 orders smaller than that in the *c*-direction [23]. This results in the nearly one-dimensional diffusion of Li^+ ions in rutile [20,21]. Consequently, the diffusion into 3D volume is greatly restricted, leading to poor performance for bulk rutile TiO_2 materials.

Recently, a number of reports suggested that nanosized rutile TiO_2 possesses significantly improved lithium intercalation capability [22,26]. This statement was further reinforced by the experimental observations that nanostructured rutile TiO_2 exhibits enhanced lithium storage performance [13,27–29]. In this communication, we report that ultra-fine rutile TiO_2 nanoparticles with only 3 nm in size, synthesized by a simple wet-chemical method followed by annealing in air, manifest superior lithium storage properties with long term cycling stability and high rate performance. While considering the ease of preparation in large scale, these ultra-fine rutile TiO_2 nanoparticles are very promising as the anode material for high-power LIB.

2. Experimental

2.1. Materials preparation

Ultra-fine rutile TiO_2 nanoparticles were synthesized by a wet-chemical method reported previously [30,31]. In a typical synthesis, 4 ml of titanium tetrachloride was added dropwise into a solution containing 100 ml of ultra-pure water and 4 ml of 37% HCl under vigorous stirring. Afterwards, the solution was kept at 60 °C for 3 h then at room temperature for approximately 15 h. The white product was then collected via centrifugation and washed thoroughly with ultra-pure water before being dried at 60 °C overnight. Thus obtained nanoparticles have a mean crystallite size of about 2 nm (denoted as TO-RT). To generate rutile nanoparticles with larger sizes, the as-prepared white powder was annealed in air at 200 °C (TO-200) and 400 °C (TO-400) for 1 h, using a ramping rate of 5 °C min^{-1}.

* Corresponding author. Tel.: +65 6316 8879; fax: +65 6791 1761.
E-mail address: xwlou@ntu.edu.sg (X.W. Lou).

0378-7753/$ – see front matter © 2009 Elsevier B.V. All rights reserved.
doi:10.1016/j.jpowsour.2009.11.040

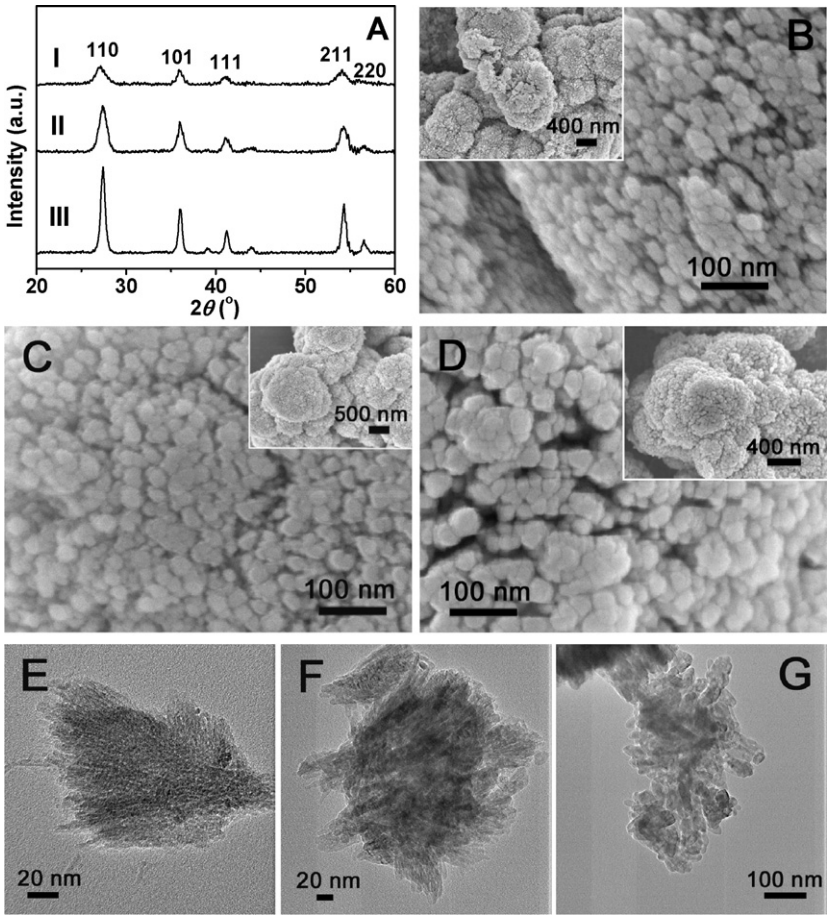

Fig. 1. (A) XRD patterns of the as-prepared rutile TiO_2 nanoparticles: TO-RT (I), TO-200 (II) and TO-400 (III). FESEM images of TO-RT (B), TO-200 (C), and TO-400 (D). The insets show the corresponding low-magnification FESEM images. (E–G) TEM images of TO-RT, TO-200, and TO-400 respectively.

2.2. Materials characterizations

Samples were characterized using X-ray power diffraction (XRD; Bruker, D8-Advance X-ray Diffractometer, Cu Kα, λ = 1.5406 Å), field-emission scanning electron microscopy (FESEM; JEOL, JSM-6700F, 5 kV), Brunauer–Emmett–Teller (BET; Quantachrome Instruments, Autosorb AS-6B).

2.3. Electrochemical measurements

The electrochemical measurements were performed using two-electrode Swagelok-type cells with lithium serving as both the counter and reference electrodes under ambient temperature. The working electrode was composed of 70 wt% of active material (e.g., ultra-fine rutile nanoparticles of different sizes), 20 wt% of conductivity agent (carbon black, Super-P-Li), and 10 wt% of binder (Polyvinylidene difluoride, PVDF, Aldrich). The electrode slurry was then casted on a copper disc which serves as the current collector. In each electrode, the loading of active material is about 1–2 mg. The electrolyte used was 1 M $LiPF_6$ in a 50:50 (w/w) mixture of ethylene carbonate and diethyl carbonate. Cell assembly was carried out in an Argon-filled glovebox with both moisture and oxygen contents below 1 ppm. Cyclic voltammetry (CV, 1–3 V, 0.5 mV s^{-1}) was performed using an electrochemical workstation (CHI 660C). Galvanostatic charge/discharge was performed using a battery tester (NEWAER). Various current densities were used for charge–discharge tests with 1 C equivalent to 170 mA g^{-1}.

3. Results and discussion

The XRD pattern shown in Fig. 1A confirms that the as-prepared nanoparticles annealed at different temperatures contain phase-pure tetragonal rutile TiO_2 (JCPDS No. 21-1276, S.G.: $P4_2/mnm$, a_o = 4.5933 Å, c_o = 2.9592 Å). It can be clearly seen that the TiO_2 nanoparticles without annealing (denoted as TO-RT) show much lower peak intensities compared to the other two samples, indicating its very small crystallite size. While the sample annealed at 400 °C (denoted as TO-400) has much sharper peaks compared to the one annealed at 200 °C (denoted as TO-200), suggesting its much larger particle size. Calculating the crystallite size using Scherrer's formula based on the (1 1 0) peak gives 2 nm, 3 nm, and 5.8 nm for samples TO-RT, TO-200, and TO-400, respectively. It is apparent that the annealing favors the crystallization process. From the FESEM images (Fig. 1B–D), it can be observed that three samples are shown with similar morphologies as large agglomerates. Even though the calculated sizes are only about a few nanometers, the particles displayed in the images are generally in the range of 10–20 nm. This is likely due to aggregation of ultra-fine primary nanoparticles caused by their high surface energy, which makes it difficult to distinguish the difference in size. These large aggregates of small rutile nanoparticles are also observed in the TEM images (Fig. 1E–G), where indeed the difference in primary crystallite size can be clearly revealed.

Electrochemical measurement was then performed to investigate the lithium storage properties of the as-prepared samples.

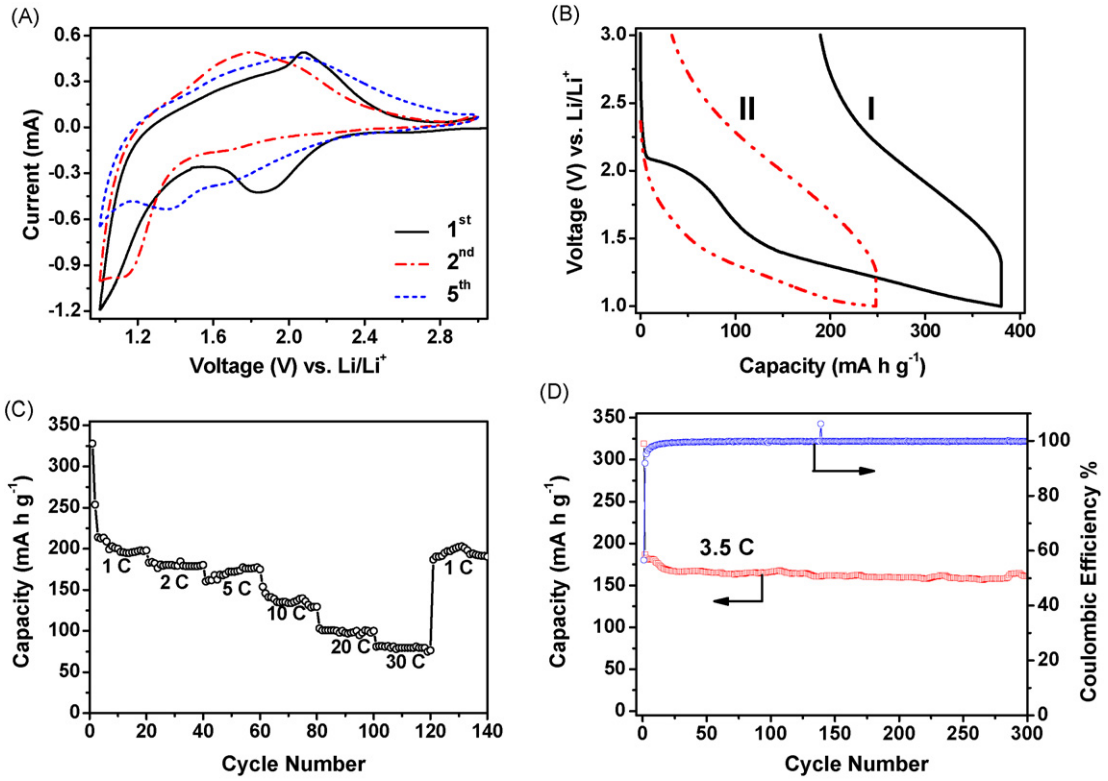

Fig. 2. Electrochemical measurements of the as-prepared rutile TiO_2 nanoparticles (TO-200). (A) Cyclic voltammograms at scan rate of 0.2 mV s^{-1}. (B) Charge/discharge voltage profiles of the first (I) and second (II) cycle at 4 C. (C) Cycling performance at different charge/discharge rates. (D) Cycling performance at a constant current drain of 3.5 C, and the corresponding Coulombic efficiency. All measurements were performed with a voltage window of 1–3 V. The discharge capacities (lithium insertion) are shown in both C and D.

Fig. 2A shows the representative cyclic voltammograms (CV) of TO-200. Generally, they are consistent with previously reported data [15,30], even thought the first set of current peaks at about 1.8 V (cathodic sweep) and 2.1 V (anodic sweep) seems to be more pronounced in the present study [13]. A more prominent cathodic peak at about 1 V can be clearly observed, which can be attributed to the lithium insertion into the rutile structure. The peak current decreases significantly in the subsequent cycles, showing the irreversible formation of $LiTiO_2$ phase from the rutile phase [13]. Its corresponding anodic peak can then be identified as a broad peak at about 1.6 V.

Fig. 2B shows the charge/discharge profile of the first two cycles of TO-200 at a current drain of 4 C. In agreement with the CV analysis, a small plateau region is observed at about 2 V during the first discharge, and the second less-defined plateau starting at about 1.4 V marks the insertion of Li^+. A high capacity of 380.2 mAh g^{-1} is delivered at the end of the discharge, and this is probably related to the high surface area (112 m^2 g^{-1}) of the rutile nanoparticles which provides more sites for lithium insertion. A much lower capacity of 190.6 mAh g^{-1} is obtained in the following charge process, leading to an irreversible capacity loss of 49.9%. Comparable initial irreversible loss was commonly observed in nanosized rutile TiO_2 [22,28,29], which is due to the large volume strain induced during lithium insertion causing trapping of Li^+ inside the structure [32]. A discharge capacity of 248.1 mAh g^{-1} is delivered in the second cycle, followed by a charge capacity of 215.1 mAh g^{-1}, giving rise to a much lower irreversible loss of only 13.3%.

Fig. 2C shows the cycling performance of TO-200 at various charge/discharge rates. Large initial capacity losses can be observed for the first few cycles, and a reversible capacity of 198.2 mAh g^{-1} is obtained at the end of 20 charge/discharge cycles at 1 C. As shown in the figure, the capacity drops steadily with the increasing current rate up to 30 C. A capacity of 76.5 mAh g^{-1} can be delivered at a high rate of 30 C. Remarkably, after cycling at 30 C, a high capacity of 187.2 mAh g^{-1} can be resumed when the current rate is reduced back to 1 C. This rate behavior is indeed comparable to that of graphene-supported nanostructured rutile TiO_2 [27,28]. The greatly enhanced lithium storage properties can be attributed to the ultra-fine particle size which leads to a very short diffusion path and a large surface area for lithium insertion/deinsertion.

Fig. 2D displays the cycling performance of TO-200 at a constant current drain of 3.5 C for 300 cycles. After a gradual loss in the course of the first 10 cycles, the capacity levels off at about 170 mAh g^{-1} throughout the cycling. At the end of 300 charge/discharge cycles, a reversible capacity of 161.1 mAh g^{-1} can still be retained with an almost 100% Coulombic efficiency throughout the cycling. The average capacity loss is thus calculated to be 0.17% per cycle, which can be considered negligible upon extended cycling. To the best of our knowledge, such a superior cycling behavior is unprecedented for rutile TiO_2 tested under similar conditions.

Post-mortem XRD analysis was carried out in order to understand the crystallographic changes induced by the lithium insertion/extraction. As shown in Fig. 3, the intensities of the two dominant peaks decrease substantially after the first discharge process, indicating that the insertion of Li^+ ions greatly affects the host structure. After the 5th discharge, the (1 1 0) peak completely disappears while the (1 0 1) peak is hardly visible. At the end of 500 charge–discharge cycles, no diffraction peaks can be identified, suggesting the loss of long-range crystal ordering. Nevertheless, local sub-1 nm ordering might still exist. More sensitive techniques are required to characterize the state of these "amorphous" Li_xTiO_2 materials.

The electrochemical properties of the other two samples were also examined. Fig. 4A shows the cycling performance of TO-RT at

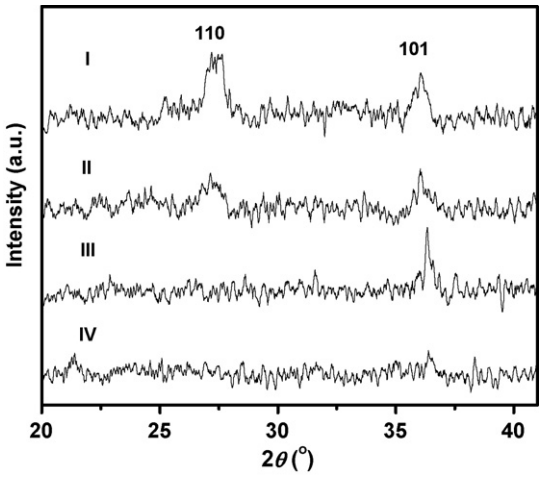

Fig. 3. XRD analysis of TO-200 after charge–discharge tests: (I) before test; (II) after 1st discharge; (III) after 5th discharge; and (IV) after 500 charge–discharge cycles. Measurements were conducted at a current rate of 1 C with a voltage window of 1–3 V.

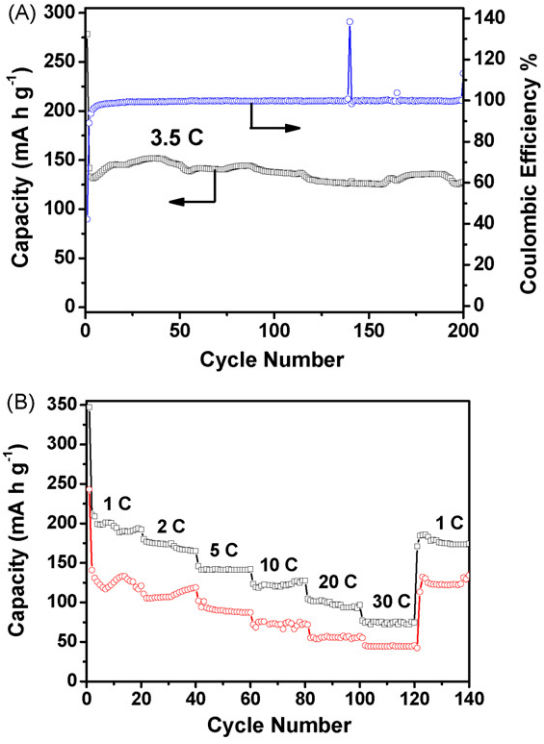

Fig. 4. (A) Cycling performance of TO-RT at a current rate of 3.5 C. (B) Rate behavior of TO-RT (□) and TO-400 (○) at different charge/discharge rates. The capacities shown are discharge capacities (lithium insertion).

3.5 C for 200 cycles. Compared to TO-200, a similarly large initial loss can be observed, and it delivers a slightly lower capacity with good capacity retention and a nearly 100% Coubombic efficiency throughout the cycling. This could be due to the fact that both samples have similar particle sizes with a very small diffusion length, allowing easy insertion/extraction of lithium. Fig. 4B compares the rate performance of TO-400 and TO-RT at various charge/discharge rates. Interestingly, TO-RT is able to give a similar rate behavior as TO-200, while TO-400 which possesses much large particle size conveys much lower capacities at all rates.

4. Conclusions

Ultra-fine rutile TiO_2 nanoparticles have been prepared following a modified simple wet-chemical method. After annealing at different temperatures in air, rutile nanoparticles with different crystallite sizes can be obtained with greatly enhanced lithium storage capabilities. Specifically, the rutile TiO_2 nanoparticles annealed at 200 °C with a mean crystallite size of only 3 nm exhibit excellent cycling performance at a high current drain of 3.5 C with a capacity loss of 0.17% per cycle over 300 cycles, as well as a good rate performance up to 30 C. The rutile TiO_2 nanoparticles obtained without annealing shows a comparable performance as the particle sizes of both samples are similar. Considering the ease of large-scale synthesis, these ultra-fine rutile nanoparticles have great potential to serve as the anode material for high-power lithium-ion batteries.

Acknowledgement

We are grateful to the Nanyang Technological University for financial support through the start-up grant (SUG).

References

[1] M. Armand, J.M. Tarascon, Nature 451 (2008) 652.
[2] P.G. Bruce, B. Scrosati, J.M. Tarascon, Angew. Chem., Int. Ed. 47 (2008) 2930.
[3] J.M. Tarascon, M. Armand, Nature 414 (2001) 359.
[4] X.W. Lou, L.A. Archer, Adv. Mater. 20 (2008) 1853.
[5] X.W. Lou, J.S. Chen, P. Chen, L.A. Archer, Chem. Mater. 21 (2009) 2868.
[6] X.W. Lou, D. Deng, J.Y. Lee, L.A. Archer, Chem. Mater. 20 (2008) 6562.
[7] X.W. Lou, D. Deng, J.Y. Lee, J. Feng, L.A. Archer, Adv. Mater. 20 (2008) 258.
[8] Z. Tao, J. Liang, J. Chen, Chem. Mater. 20 (2007) 667.
[9] X.W. Lou, Y. Wang, C.L. Yuan, J.Y. Lee, L.A. Archer, Adv. Mater. 18 (2006) 2325.
[10] X.W. Lou, L.A. Archer, Z.C. Yang, Adv. Mater. 20 (2008) 3987.
[11] Y.G. Guo, Y.S. Hu, W. Sigle, J. Maier, Adv. Mater. 19 (2007) 2087.
[12] J.W. Xu, C.H. Ha, B. Cao, W.F. Zhang, Electrochem. Acta 52 (2007) 8044.
[13] D. Wang, D. Choi, Z. Yang, V.V. Viswanathan, Z. Nie, C. Wang, Y. Song, J.-G. Zhang, J. Liu, Chem. Mater. 20 (2008) 3435.
[14] A.R. Armstrong, G. Armstrong, J. Canales, R. García, P.G. Bruce, Adv. Mater. 17 (2005) 862.
[15] L. Kavan, D. Fattakhova, P. Krtil, J. Electrochem. Soc. 146 (1999) 1375.
[16] L. Kavan, M. Gratzel, S.E. Gilbert, C. Klemenz, H.J. Scheel, J. Am. Chem. Soc. 118 (1996) 6716.
[17] M. Wagemaker, A.P.M. Kentgens, F.M. Mulder, Nature 418 (2002) 397.
[18] M. Wagemaker, R. van de Krol, A.P.M. Kentgens, A.A. van Well, F.M. Mulder, J. Am. Chem. Soc. 123 (2001) 11454.
[19] A. Stashans, S. Lunell, R. Bergström, A. Hagfeldt, S.-E. Lindquist, Phys. Rev. B 53 (1996) 159.
[20] M.V. Koudriachova, N.M. Harrison, S.W. de Leeuw, Phys. Rev. B 65 (2002).
[21] M.V. Koudriachova, N.M. Harrison, S.W. de Leeuw, Solid State Ionics 157 (2003) 35.
[22] E. Baudrin, S. Cassaignon, M. Koesch, J.P. Jolivet, L. Dupont, J.M. Tarascon, Electrochem. Commun. 9 (2007) 337.
[23] D. Deng, M.G. Kim, J.Y. Lee, J. Cho, Energy Environ. Sci. 2 (2009) 818.
[24] W.J. Macklin, R.J. Neat, Solid State Ionics 53–56 (2003) 694.
[25] M.C. Payne, M.P. Teter, D.C. Allan, T.A. Arias, J.D. Joannopoulos, Rev. Mod. Phys. 64 (1992) 1045.
[26] W.J.H. Borghols, M. Wagemaker, U. Lafont, E.M. Kelder, F.M. Mulder, Chem. Mater. 20 (2008) 2949.
[27] D.H. Wang, D.W. Choi, J. Li, Z.G. Yang, Z.M. Nie, R. Kou, D.H. Hu, C.M. Wang, L.V. Saraf, J.G. Zhang, I.A. Aksay, J. Liu, ACS Nano 3 (2009) 907.
[28] Y.S. Hu, L. Kienle, Y.G. Guo, J. Maier, Adv. Mater. 18 (2006) 1421.
[29] C.H. Jiang, I. Honma, T. Kudo, H.S. Zhou, Electrochem. Solid State Lett. 10 (2007) A127.
[30] N.A. Milne, M. Skyllas-Kazacos, V. Luca, J. Phys. Chem. C 113 (2009) 12983.
[31] M. Anpo, T. Shima, S. Kodama, Y. Kubokawa, J. Phys. Chem. 91 (1987) 4305.
[32] M. Vijayakumar, S. Kerisit, C.M. Wang, Z.M. Nie, K.M. Rosso, Z.G. Yang, G. Graff, J. Liu, J.Z. Hu, J. Phys. Chem. C 113 (2009) 14567.